# Development and Comparison of ANN-LM and ANN-BR Models for Predicting the Performance of Membrane Based Novel Liquid Desiccant Drying/Air Conditioning cum Desalination System

Tryambke Pandey[1], P. K. S. Tejes[1], *B. Kiran Naik[1]

Author Affiliations

[1]*Sustainable Thermal Energy Systems Laboratory (STESL), Department of Mechanical Engineering, National Institute of Technology Rourkela, Odisha–769008, INDIA,*

*Author Emails*

**Corresponding author: k.bukke@gmail.com; naikkb@nitrkl.ac.in; Ph. No.: +919435686059*

**Abstract.** The major issue in extracting pure water from humid air is design of energy-efficient dehumidifier and regenerator as well as optimization of the working processes. In the current study, a novel liquid desiccant air conditioning/drying cum desalination system is analyzed by incorporating M-cycle based dehumidification and flat plate type polyvinylidene difluoride (PVDF) membrane-based indirect contact regenerator has been proposed which is investigated by using two artificial neural network (ANN) models i.e., Levenberg-Marquardt (ANN-LM) and Bayesian Regularization (ANN-BR). To investigate the model three different activation functions i.e., Tangent Sigmoid in both layers, Tangent Sigmoid & Linear, and Logarithmic Sigmoid & Linear for hidden and output layers are applied using experimental data from the literature. To perform the numerical analysis four inlet parameters (mass flow rate of water and liquid desiccant, liquid desiccant concentration at inlet, regenerator inlet temperature of water, and liquid desiccant) is considered to predict three-outlet parameters which are pure water extraction rate, liquid desiccant regenerator outlet concentration, and liquid desiccant regenerator outlet temperature. These combinations are explored and it has been established that ANN-LM with activation function Tan-Sigmoid + Tan-Sigmoid is the best performing combination having $R^2$ value of 0.98 for pure water extraction rate, 0.97 for liquid desiccant solution concentration, and 0.99 for liquid desiccant outlet temperature. It has also been observed that a combination of ANN-BR with activation function Log-Sigmoid + Linear was the least accurate for predicting the exit parameters. The predicted values have been found to be in excellent concurrence with the experimental data.

## 1. INTRODUCTION

Development of the agricultural sectors and increase in demand for human comfort has resulted in a rise in high productivity and better air quality. In regions with high relative humidity such as in coastal zones, integrated Maisotsenko cycle (M-Cooler) based indirect (polyvinylidene fluoride hydrophobic membrane) contact dehumidifier (MCID) can be chosen as an alternative over the conventional structured based dehumidifier because of low energy consumption, ease of fabrication, low maintenance cost and capability to remove bacteria and virus [1], etc. The use of liquid desiccant (LD) dehumidification/desalination system has several promising advantages including effective utilization of industrial waste heat [2,3], low-quality energy, and renewable energy e.g., wind energy [4], solar energy [5,6]. The earlier developed liquid desiccant air conditioning systems (LACS) had certain drawbacks as due to direct interaction between liquid desiccant and air there is a chance of desiccant carryover with air which tends to corrode the air duct, room furniture, walls also may damage to the health of people in air conditioning space and may spoil perishable goods in the drying chamber, hence in this study a flat plate membrane-based type indirect evaporative cooler is used where liquid desiccant i.e., Lithium chloride (LiCl) and air are separated by a flat plate hydrophobic PVDF (polyvinylidene fluoride) membrane is used which facilitates the exchange of mass and energy simultaneously with high efficacy and notable pressure drop. In dehumidifier, the liquid desiccant absorbs water vapour. The main driving force causing the energy and mass exchange to occur are temperature and vapour pressure gradient at the air-liquid desiccant boundary. Although air gets dehumidified in the

conventional system yet the exit air temperature of the dehumidifier is low which makes it incapable of drying purposes; even air that is being released into the atmosphere is almost saturated which could have been used to extract pure water.

With the intention of predicting the performance of the system transport phenomena and thermodynamic properties are considered however predicting all possible combinations is difficult. In order to counteract this limitation, a data-driven approach can be implemented to accurately predict using artificial intelligence-machine learning (AI-ML) [12]. Artificial neural network (ANN) is extensively employed for solving complex systems. There are several types of learning algorithms such as Quasi-Newton algorithms, Conjugate gradient algorithms (CG), Bayesian regularization (BR), and Levenberg-Marquardt (LM) are most commonly used [13-20]. Quasi-Newton gives much faster results but they are more prone to memory loss [13]. ANN-LM is quicker without getting trapped with local minima [14-17]. The disadvantage associated with ANN-LM is that it suffers from low convergence while minimizing a nonlinear least-squares function [18]. ANN-BR is more robust compared to any other back-propagating algorithm. Overtraining and overfitting are avoided in ANN-BR nevertheless weight of the network [19]. BR comparatively takes less time than LM. ANN has gained popularity in recent years for predicting and optimization for energy application [20-22] humidification-dehumidification systems [23-25], performance of membrane [26], and cavitation [27].

As per the reported literature, it is evaluated that numerous thermal models have been proposed by researchers for evaluating the direct interaction-based structured packing chamber using LD during dehumidification-regeneration performance [1-10]. Very limited researchers proposed thermal models for investigating the membrane-based LD dehumidification-regeneration performance [11-18]. Few investigators have presented thermal models for investigating the conventional LDAC system performance (direct contact structured packing chamber-based LDAC system) [14, 19-24]. Moreover, limited thermal models were developed for analyzing membrane-based conventional LDAC system performance [16, 25-27]. Further, very few researchers analyzed the performance of the conventional LDAC system for drying cum desalination purposes [18, 27]. Furthermore, it is obvious from the literature that there is a deficit in thoughtful research on the suggested LDAC/drying cum desalination system by incorporating Maisotsenko cycle-based M-cooler during the dehumidification process.

With respect to the above-mentioned, the current study explores a novel multipurpose LD air conditioning/drying cum desalination system by incorporating Maisotsenko cycle (M-Cooler) based indirect (polyvinylidene fluoride hydrophobic membrane) contact dehumidifier (MCID) and by employing indirect contact-based membrane technology for pure water extraction rate ($\sigma$) as well as flat plate polyvinylidene difluoride (PVDF) membrane-based indirect contact regenerator with water in place of air. For predicting pure water extraction rate ($\sigma$), LD outlet solution concentration ($X_{d,o}$), and outlet temperature ($T_{d,o}$) two different backpropagating algorithms are proposed, which are ANN-based LM and BR using three different activation functions, which are Tan sigmoid in both layers, Tan sigmoid & Linear, and Logarithmic Sigmoid & Linear in hidden and output layer, respectively. The ANN model comparison is done using statistical criteria $R^2$, MAE, MAPE, and RMSE for both training and testing data. The novelty of the present work is associated not only with the design of the MCID and restructuring of the regenerator but also with the use of AI-ML modelling for analyzing the relationship and validation of the novel system. In this article, both the challenges i.e., optimal design of the system and analysis based on AI-ML have been addressed simultaneously.

## 2. NOVEL SYSTEM CYCLE

The proposed multipurpose novel system cycle has two applications, they are air conditioning cum desalination and drying cum desalination applications as shown in FIGURE 1. The variation of desiccant concentration with vapour pressure for the novel model is shown in FIGURE 2. In the proposed model, the integrated Maisotsenko cycle (M-Cooler) based indirect (polyvinylidene fluoride hydrophobic membrane) contact dehumidifier (MCID) is used in place of structured packing chamber-based direct contact dehumidifier and cooling chamber for improving the dehumidification capacity (FIGURE 2 and 3a). Whereas flat plate polyvinylidene fluoride (PVDF) hydrophobic membrane-based indirect contact regenerator is proposed as an alternative to the structured packing chamber based direct contact regenerator and water is used in place of ambient air as a working fluid at the LD regenerator for extracting fresh/pure water vapour from the weak LD through the hydrophobic membrane (FIGURE 2 and 3b). Further, lithium chloride is used as an LD for the performance assessment of conventional and novel systems. LiCl is preferred as it is the most reliable and chemically stable liquid desiccant due to its virtue of low vapour pressure

during the dehumidification and regeneration process. In addition, it is easier to compare conventional and novel systems, due to previously carried out research using LiCl.

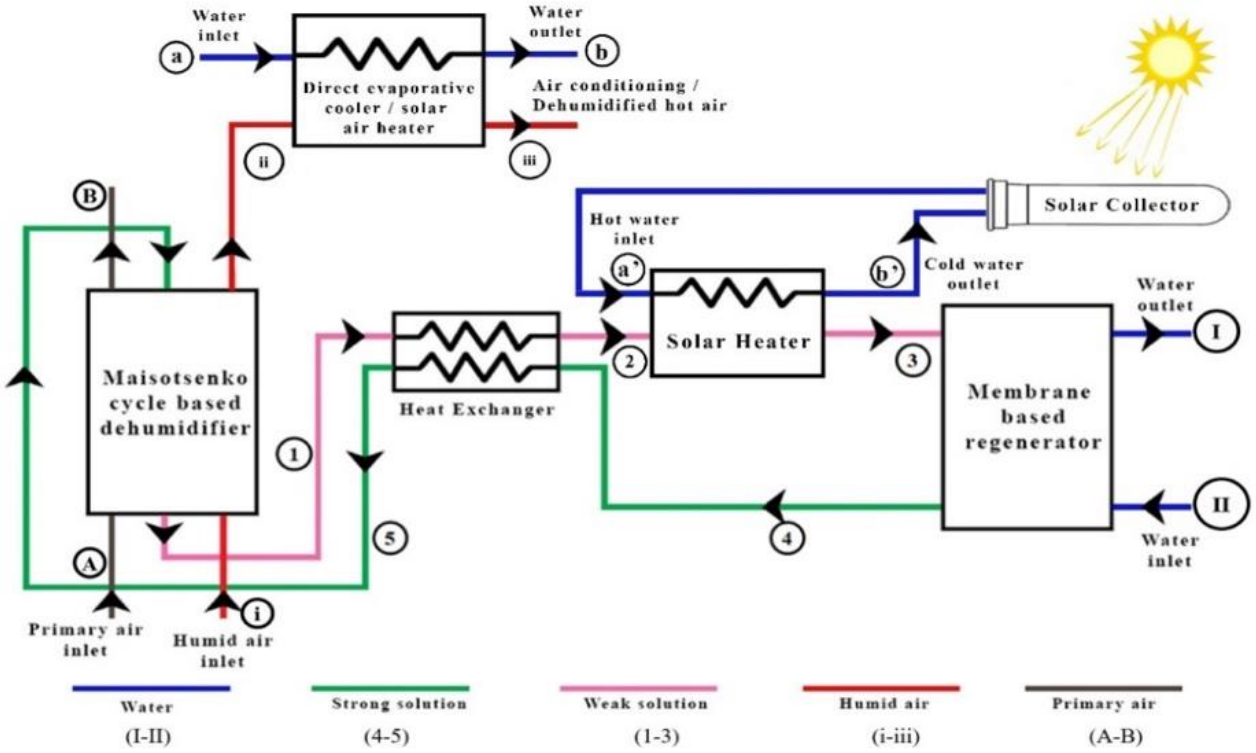


**FIGURE 1.** Schematic of proposed M-Cooler based novel air conditioning/drying cum desalination system.

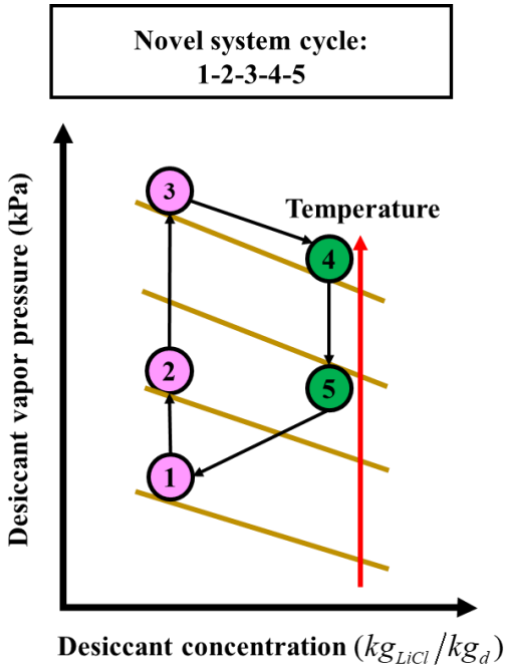


**FIGURE 2.** Vapour pressure variation with LD for novel system.

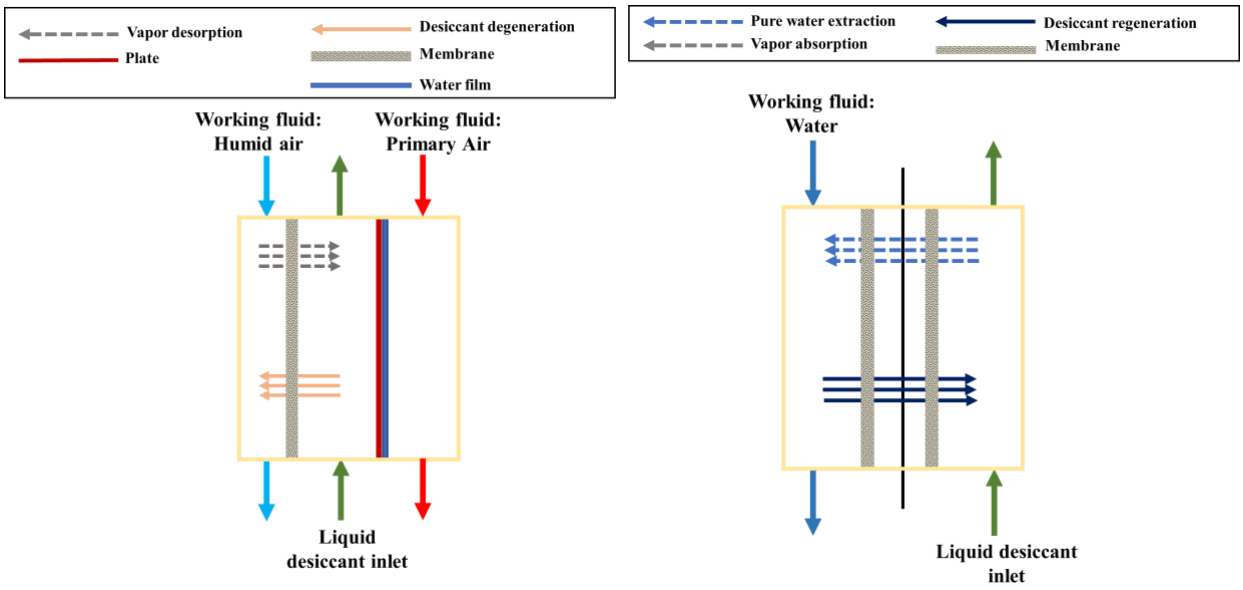


(a) Dehumidifier (b) Regenerator

**FIGURE 3.** Schematics of dehumidifier and regenerator in the novel system.

## 2.1. Importance of M-Cooler

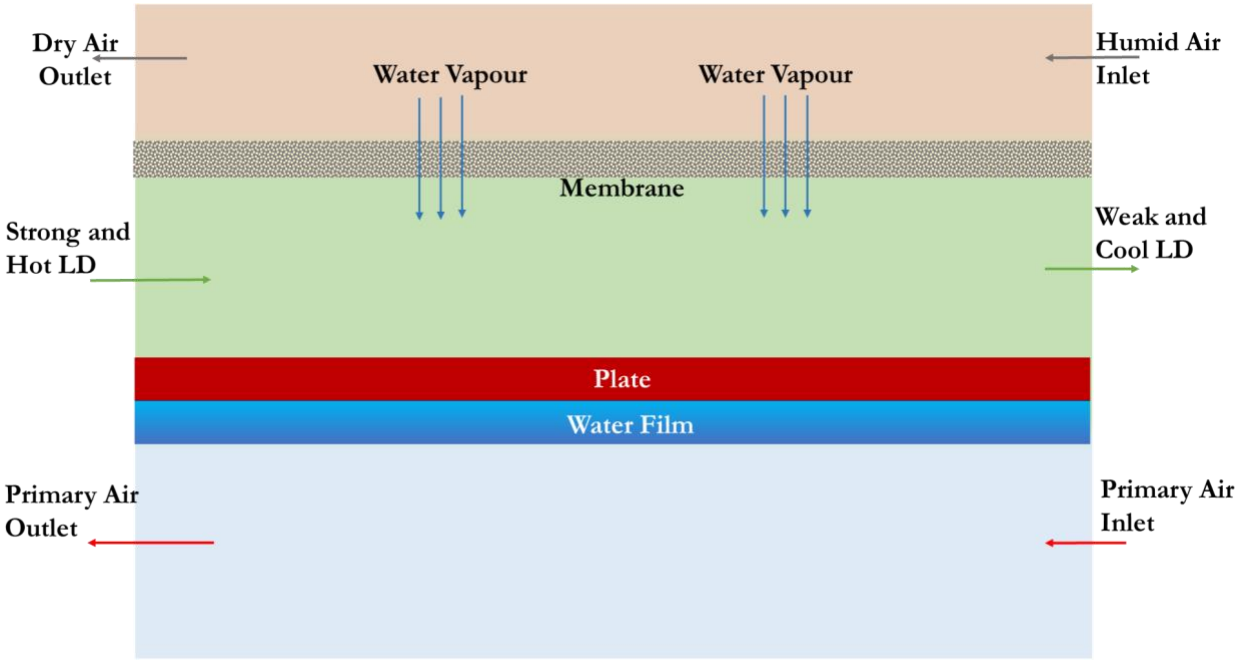


**FIGURE 4.** Internal structure of the MCID.

The MCID present in the novel system has three loops (FIGURE 1 and 2a), they are humid air loop (i–iii), primary air loop (A–B), and LD loop (5–1). The detailed schematic of the MCID internal structure is illustrated in FIGURE 4. In the humid air loop (i–iii), the humid air enters the dehumidifier in a counter flow direction, and it is in

indirect interaction with the strong and hot LD through the PVDF-based hydrophobic membrane. When the humid air comes in indirect contact with the LD, moisture removal from the humid air occurs due to vapour pressure and temperature gradients as well as an exothermic reaction. In MCID, incorporating membrane in the dehumidifier eradicates the carryover and improves the vapour absorption rate due to the hydrophobic nature of the membrane (i.e., only water vapour can penetrate through the membrane from humid air to the LD). In the primary air loop (A–B), the primary air and water with one another are interacted in opposite directions. During this encounter, the evaporation of water film occurs resulting in lowering the water temperature. This phenomenon leads to cooling the LD which is in indirect contact with the water through a stainless-steel plate. In the LD loop (5–1), the LD comes in indirect contact with the cold water and humid air which are separated by the plate and membrane, respectively. Thus, the hot and strong LD entering the MCID converts to cold and weak LD.

## 2.2. Dehumidified Air for Air Conditioning and Drying Applications

In the present investigation, the usage of dehumidified air for AC and drying applications are explored to elevate the performance of the conventional air conditioning and drying systems in humid climates. In the present study, dehumidified air is passed through the DEC and solar heater for air conditioning and drying applications, respectively (FIGURE 1). For air conditioning applications, dehumidified air is cooled and humidified to the desired comfort conditions by interacting with the water flowing in opposite direction. Here, the cold and humidified air are achieved due to the evaporative cooling process (FIGURE 1). For drying application, the dehumidified air is made to pass through a solar air heater to raise the temperature (heat) of the dehumidified air to the required conditions (FIGURE 1).

## 2.3. ANN-AI Tool

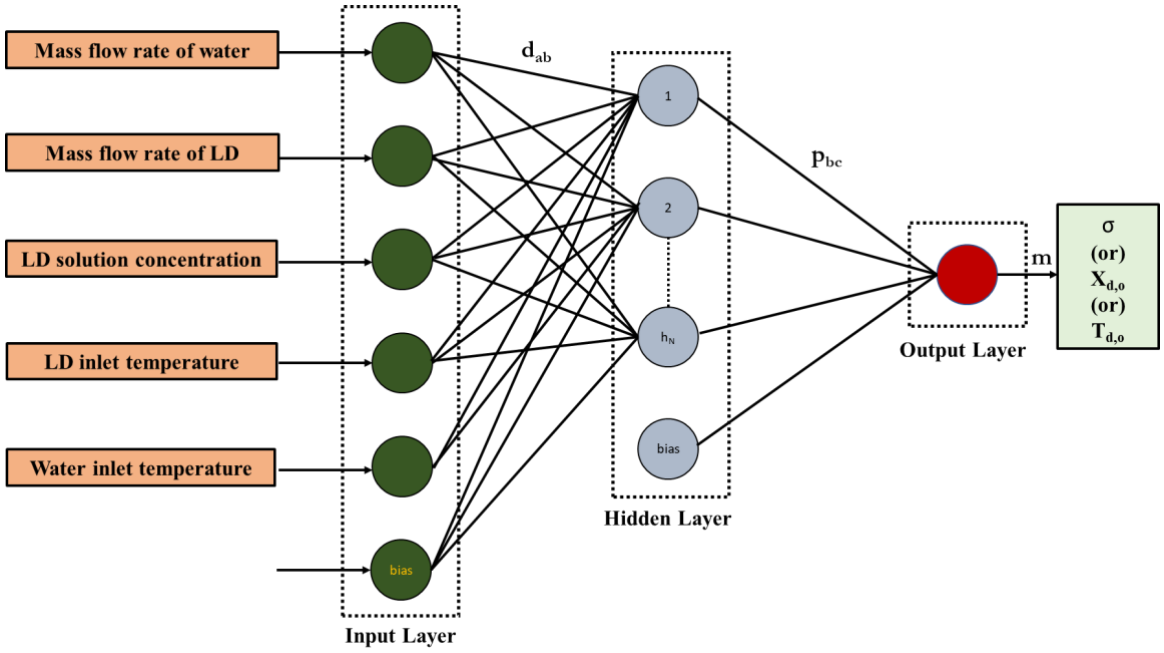


**FIGURE 5.** Proposed single hidden layer ANN model structure.

As per the reported literature [28] artificial intelligence tool such as artificial neural network (ANN-AI) has been used as an efficient learning algorithm out of which ANN-LM (Levenberg-Marquardt) and ANN-BR (Bayesian Regularization) have been confirmed to be very strong and quick learning algorithms when compared to others, such as Conjugate Gradient (CG) and Quasi-Newton. In the current study, two back-propagation learning algorithms, which are ANN-LM and ANN-BR are used along with three activation functions which are tangent sigmoid, logarithmic sigmoid, and linear transfer function to calculate the three outlet parameters (pure water extraction rate

(σ), LD outlet temperature ($T_{d,o}$) and water outlet temperature ($T_{w,o}$)) using five inlet parameters (mass flow rate of water & LD, solution concentration of LD, inlet temperature of LD and water). The study consisting of these six combinations of a learning algorithm in the hidden and output layer, respectively i.e., ANN-LM (Tan sigmoid in both layers), ANN-LM (Tan sigmoid & Linear), ANN-LM (Log sigmoid & linear), ANN-BR (Tan sigmoid in both layers), ANN-BR (Tan sigmoid & Linear), and ANN-BR (Log sigmoid & linear) are explored. The single hidden layer for the above-mentioned model is presented in FIGURE 5. In the present analysis, inputs of the targeted network are scaled in the range of ±5 whereas the output is scaled in the range of ±1. This is done in order to bring the input and output data to a common magnitude. The mathematical depiction of the six explored ANN models is discussed below,

Input: $$N = [l_1, l_2 \ldots\ldots\ldots\ldots l_n] \quad (1)$$

where, 'N' is the input taken which varies from '$l_1$' to '$l_n$', and n is the number of inputs taken.
Scaling of input is done as,

Scaling of input: $$S_a = \left\{\left(\frac{N_a - N_a^{min}}{N_a^{max} - N_a^{min}}\right) X10\right\} - 5 \qquad a = 1,2,3,....n \quad (2)$$

where, '$S_a$' depicts the scaling of the input at 'a'. $N_n^{max}$, and $N_n^{min}$ is the maximum and minimum limit of inputs based on the range of pertinence of the model.
$H_b$ is the hidden layer input at the $b^{th}$ neuron, it is represented as,

Hidden layer input: $$H_b = \sum_{a=1}^{n} S_a d_{ab} + d_{0b} \qquad b = 1,2,3,.....h_d \quad (3)$$

where, '$h_d$', is the number of neurons present in the hidden layer, '$d_{ob}$' and '$d_{ab}$' denote the weight of input bias neuron attached to the $b^{th}$ neuron and $a^{th}$ neuron, respectively.

Hidden layer output for Tan-Sigmoid: $$\lambda_b = \left(\frac{2}{1+\exp(-2\times H_b)}\right) - 1 \qquad b = 1,2,3,.....h_d \quad (4)$$

Hidden layer output for Log-Sigmoid: $$\lambda_b = \left(\frac{1}{1+\exp(-H_b)}\right) \qquad b = 1,2,3,.....h_d \quad (5)$$

where, '$\lambda_b$' is the hidden layer output at the '$b^{th}$' neuron using Tan Sigmoid and Log Sigmoid function as shown in Eqs. 4 and 5, respectively.

Output layer at $c^{th}$ neuron: $$\gamma_n = \sum_{b=1}^{c} \lambda_b p_{bc} + p_{0c} \qquad c = 1,2,3,.....out \quad (6)$$

where, '$p_{oc}$' represents hidden bias neuron weight associated with the $c^{th}$ neuron in the output layer, and '$p_{bc}$' depicts the hidden bias neuron weight associated to with the $c^{th}$ neuron and $b^{th}$ neuron present in the in output and hidden layer, respectively, 'out' is the number of outputs present.

Output for Tan-Sigmoid: $$\lambda_c = \left(\frac{2}{1+\exp(-2\gamma_c)}\right) - 1 \qquad c = 1,2,3,.....out \quad (7)$$

Output for Log-Sigmoid: $$\lambda_c = \left(\frac{1}{1+\exp(-\gamma_c)}\right) \qquad c = 1,2,3,.....out \quad (8)$$

Output for Linear: $$\lambda_c = \gamma_c \qquad c = 1,2,3,.....out \quad (9)$$

In the output i.e., '$\lambda_c$', for the $c^{th}$ neuron can be calculated using the Eqs. 7-9 for Tan Sigmoid, Log Sigmoid, and linear function respectively.
To calculate the $c^{th}$ neuron descaling can be done as,

Descaling of output: $$m_c = m_{min} + \left(\frac{\lambda_c + 1}{2}\right) \times \left(m_{max} - m_{min}\right) \qquad c = 1,2,3,.....out \quad (10)$$

$$\alpha = \begin{bmatrix} d_{ab}; a = 0,1,2,.....n \,\&\, b = 0,1,...,h_d \\ d_{0b}; b = 0,1,2,.....h_d \\ p_{bc}; b = 0,1,2,.....h_d \,\&\, c = 0,1,...,out \\ p_{0c}; c = 0,1,2,.....out \end{bmatrix} \quad (11)$$

where, 'α' represent the total weight of the network
ANN-LM algorithm [29] can be represented as,

Levenberg-Marquardt: $$\omega_{k+1} = \omega_k + \left(J_k^T J_k + \nu I\right)^{-1} J_k e^k \quad (12)$$

where, ν is combination coefficient, ω is weight vector, 'I' is the identity matrix, J and $J^T$ are Jacobian and its transpose.
ANN-BR algorithm [30] can be represented as,

Bayesian-Regularization: $$\psi(w) = \gamma \sum_{i=1}^{g} [y_i - f(x_i)]^2 + \Theta \sum_{j=1}^{h} w_j^{\,2} \quad (13)$$

where, 'h' is the number of weights, $\gamma$ and Θ are hyperparameters, 'g' is number of rows, ψ is minimized with respect to 'w' weight.
Learning algorithm, ANN-LM [29] (Eq. 12) and ANN-BR [30] (Eq. 13) have been adopted in order to predict the output (Eqs. 6–11) in terms of input (Eqs. 1–3) through hidden layers (Eq. 4 and 5).

## 2.4. Error Prediction Measures

To analyze the performance of the model during training and testing in the current study statistical parameters are chosen which are coefficient of determination ($R^2$), mean absolute error (MAE), mean absolute percentage error (MAPE), and root mean square error (RMSE) are considered. To depict strong relation between the input variables a closer value of 1 is desired. 0 depicts no correlation whereas 0.5 indicates moderate correlation. In the case of MAE, MAPE, and RMSE value closer to 0 is considered a better model. In order to calculate the respective values following correlations are used,

Coefficient of determination: $$R^2 = 1 - \frac{\sum_{i=1}^{N} (X_i - X_i)^2}{\sum_{i=1}^{N} (X_i - \overline{X_i})^2} \quad (14)$$

Mean absolute: $$MAE = \frac{1}{N} \sum_{i=1}^{N} | X_i - X_i | \quad (15)$$

Mean absolute percentage error: $$MAPE = \frac{1}{N} \sum_{i=1}^{N} \left( \frac{\left| X_i - X_i \right|}{X_i} \right) * 100 \quad (16)$$

Root mean square error: $$RMSE = \sqrt{\frac{\sum_{i=1}^{N} (X_i - X_i)^2}{N}} \quad (17)$$

where $\overline{X_i}, X_i, X_i$, and N are mean value of experimental dataset, predicted value, experimental data, and number of samples.

## 3. RESULTS AND DISCUSSIONS

As mentioned in the previous section, two AI-ML models, which are ANN-LM and ANN-BR are applied using three different types of activation function, which are Tan-Sig + Tan-Sig, Tan-Sig+ Linear, and Log-Sig + Linear using experimental data available in the literature [3]. These six models emanated through the combination of two backpropagation learning algorithms with three abovementioned activation functions are formed. The operating range for the five inlet parameters, which are mass flow rate of water & LD, solution concentration of LD, inlet temperature of LD, and water are mentioned in Table 1. Furthermore, in order to develop the model, the dataset is distributed into a ratio of 70:15:15 for training – testing – validation, respectively. In TABLE 2, hyperparameters for

all the three models for the prediction of pure water extraction rate, LD outlet temperature, and water outlet temperature are mentioned. In order to obtain the optimal criteria $R^2$ should be closer to 1 whereas MAE, MAPE, RMSE should be minimum. Performance comparison of which is illustrated in FIGURE 6 in combination with TABLE 3.

**TABLE 1.** Input parameters and experimental data range [3].

| Parameters | Mass flowrate of water (mL/min) | Mass flowrate of LD (mL/min) | LD solution concentration ($kg_{LiCl}/kg_{sol}$) | LD inlet temperature (°C) | Water inlet temperature (°C) |
|---|---|---|---|---|---|
| Range | 50-100 | 150-200 | 0.3-0.4 | 62-65 | 17-20.2 |

**TABLE 2.** LM and BR hyperparameters.

| Parameters | Tan-S + Tan-S | Tan-S + Linear | Log-S + Linear |
|---|---|---|---|
| Hidden layer neurons | 8 | 8 | 8 |
| Maximum epochs | 1000 | 1000 | 1000 |
| Minimum gradient | 1.00e-7 | 1.00e-7 | 1.00e-7 |
| Training algorithm | ANN-LM &ANN-BR | ANN-LM &ANN-BR | ANN-LM &ANN-BR |

**TABLE 3.** Performance comparison of ANN models.

| | | | Pure water extraction rate | | | LD outlet concentration | | | LD outlet temperature | | |
|---|---|---|---|---|---|---|---|---|---|---|---|
| Error | Algorithm | | Tan-S + Tan-S | Tan-S + Linear | Log-S + Linear | Tan-S + Tan-S | Tan-S + Linear | Log-S + Linear | Tan-S + Tan-S | Tan-S + Linear | Log-S + Linear |
| $R^2$ | ANN-LM | Train | 0.98 | 0.96 | 0.92 | 0.97 | 0.95 | 0.90 | 0.99 | 0.96 | 0.87 |
| | | Test | 0.97 | 0.95 | 0.90 | 0.97 | 0.95 | 0.89 | 0.98 | 0.95 | 0.86 |
| | ANN-BR | Train | 0.96 | 0.92 | 0.89 | 0.96 | 0.94 | 0.91 | 0.97 | 0.93 | 0.89 |
| | | Test | 0.94 | 0.90 | 0.88 | 0.96 | 0.93 | 0.90 | 0.97 | 0.91 | 0.88 |
| MAE | ANN-LM | Train | 0.027 | 0.045 | 0.049 | 0.011 | 0.055 | 0.030 | 0.038 | 0.046 | 0.056 |
| | | Test | 0.029 | 0.047 | 0.052 | 0.012 | 0.059 | 0.036 | 0.040 | 0.048 | 0.058 |
| | ANN-BR | Train | 0.049 | 0.059 | 0.066 | 0.022 | 0.075 | 0.054 | 0.076 | 0.089 | 0.095 |
| | | Test | 0.054 | 0.061 | 0.069 | 0.024 | 0.079 | 0.060 | 0.079 | 0.091 | 0.097 |
| MAPE | ANN-LM | Train | 0.620 | 1.040 | 1.000 | 1.440 | 2.102 | 2.054 | 0.420 | 0.650 | 0.880 |
| | | Test | 0.643 | 1.070 | 1.030 | 1.654 | 2.295 | 2.089 | 0.620 | 0.780 | 0.940 |
| | ANN-BR | Train | 0.840 | 1.784 | 1.345 | 1.890 | 2.700 | 2.400 | 0.400 | 0.784 | 0.850 |
| | | Test | 0.890 | 1.988 | 1.556 | 2.260 | 3.263 | 2.930 | 0.560 | 0.890 | 1.000 |
| RMSE | ANN-LM | Train | 0.038 | 0.064 | 0.061 | 0.010 | 0.014 | 0.022 | 0.027 | 0.056 | 0.042 |
| | | Test | 0.044 | 0.068 | 0.063 | 0.011 | 0.015 | 0.024 | 0.029 | 0.058 | 0.045 |
| | ANN-BR | Train | 0.078 | 0.088 | 0.095 | 0.018 | 0.026 | 0.086 | 0.049 | 0.059 | 0.079 |
| | | Test | 0.081 | 0.092 | 0.097 | 0.019 | 0.029 | 0.088 | 0.055 | 0.068 | 0.098 |

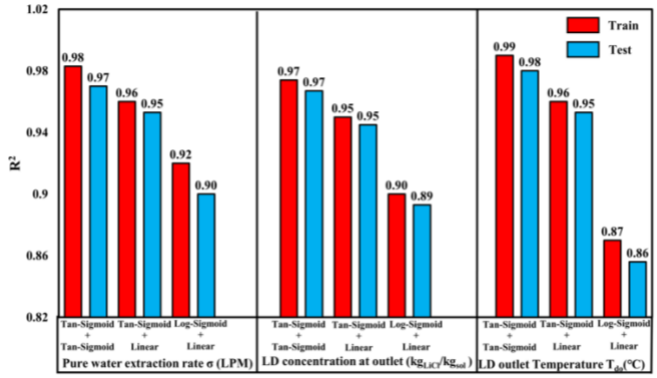


a. $R^2$ for ANN-LM activation function

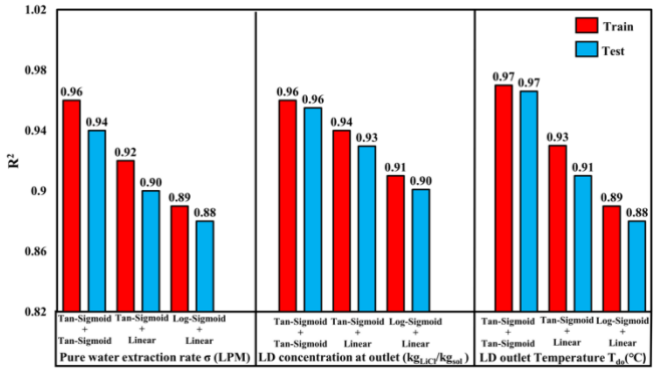


b. $R^2$ for ANN- BR activation function

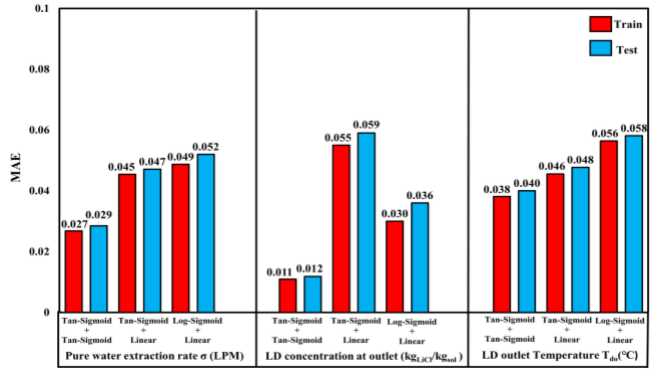


c. MAE for ANN-LM activation function

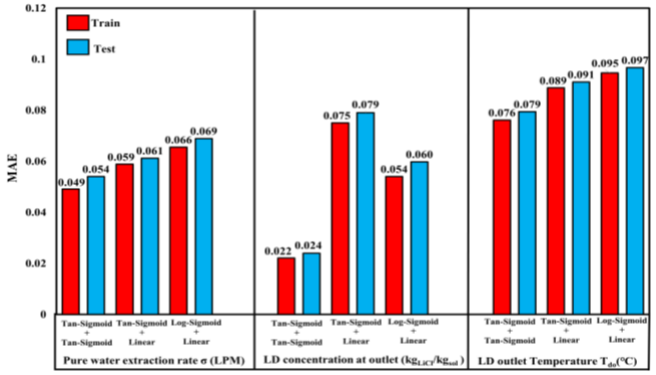


d. MAE for ANN- BR activation function

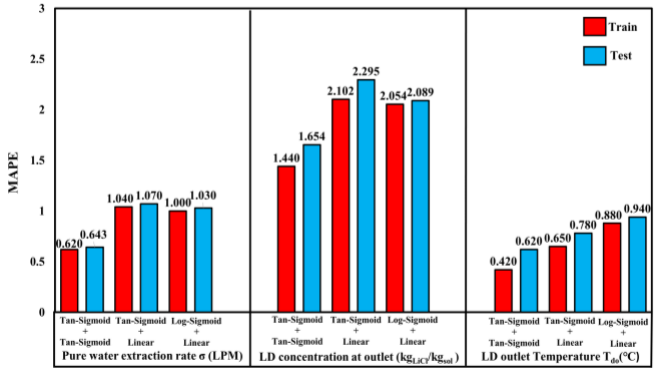


e. MAPE for ANN-LM activation function

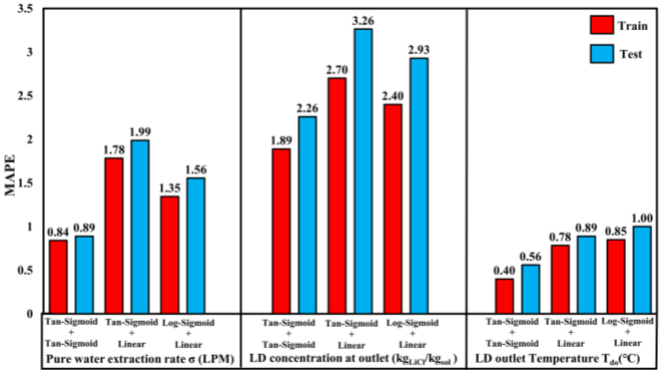


f. MAPE for ANN- BR activation function

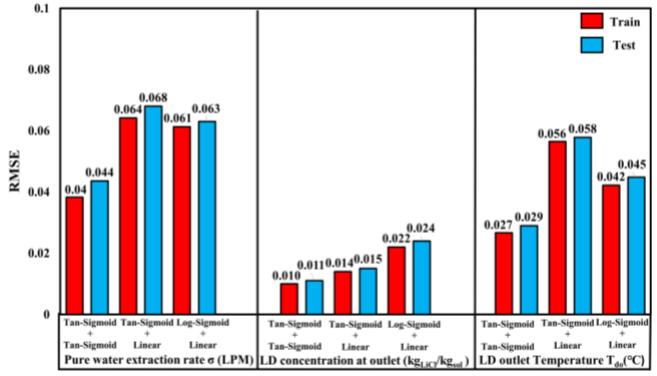


g. RMSE for ANN-LM activation function

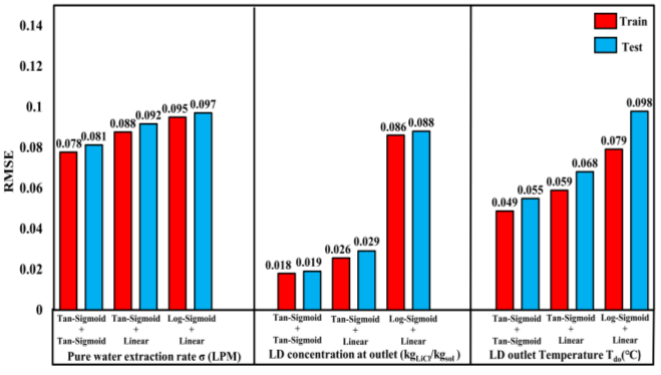


h. RMSE for ANN-BR activation function

**FIGURE 6.** Performance comparison of ANN-LM and ANN-BR using different statistical criteria.

Fig. 6a and 6b represent the comparison of coefficient of determination ($R^2$) (Eq. 14) between ANN-LM and ANN-BR based on the data evaluated in TABLE 3. Figs. 6c–6h illustrates the comparison of errors i.e., MAE, MAPE, and RMSE (Eqs. 15–17) which is evaluated for both the learning algorithms i.e., ANN-LM and ANN-BR, and three activation functions based on the data provided in TABLE 3. It can be observed from the comparison shown between ANN-LM and ANN-BR that the best performing combination of ANN model and activation function for pure water extraction rate is ANN-LM and Tan-Sigmoid in both layers since the value of $R^2$ is 0.99 which is highest whereas the MAE, MAPE, and RMSE are lowest with the value of 0.027, 0.62, and 0.038, respectively is minimum in this case. For LD outlet temperature and concentration Tan-Sigmoid in both the layers is the best performing combination with $R^2$ 0.97 and 0.99, respectively. It can be also be observed that the least-performing model is ANN-BR with activation function of Log-Sigmoid + Linear for predicting pure water extraction rate and outlet temperature of LD, whereas in the case of LD solution concentration at the outlet the ANN-BR with activation function of Tan-Sigmoid + Linear is the least accurate combination.

## 4. CONCLUSION

Extraction of pure water is dependent on the design and optimization of a high-energy efficient dehumidifier and regenerator. Hence, the present study is an approach for predicting and designing MCID and membrane-based indirect contact regenerator using artificial intelligence-machine learning (AI-ML) tool to extract the maximum amount of pure water from the inlet humid air. After a thorough investigation of the available literature in the past decade, two algorithms are selected which are Bayesian Regularization (ANN-BR) and Levenberg-Marquardt (ANN-LM). These two algorithms are used in combination with three different activation functions which are Tan-S in both layers, Tan-S & L, and Log-S & Linear for hidden and output layers. It has been found that 8 neurons for the statistical measures i.e., $R^2$, MAE, MAPE, and RMSE were observed to be optimum in the hidden layers. After analyzing all the six combinations it has been found that LM-based ANN with activation function Tan-Sigmoid in both layers is the best performing combination for predicting the pure/freshwater extraction rate, LD concentration, and LD outlet temperature with $R^2$ 0.98, 0.97, and 0.99, respectively. Furthermore, it has been also found that the predicted data is in good agreement with the experimental dataset. The present study showcases a novel approach towards dehumidifier and regenerator systems using AI and ML tools and opens a new pathway for investigators to apply the aforementioned system and AI-ML tools for analyzing mass and energy exchange system for the advancement of LD based air conditioning/drying systems for extracting pure water from humid air.

## ACKNOWLEDGMENTS

This work is carried out as a part of the ongoing technology development project entitled “Development of Novel Multipurpose Liquid Desiccant Drying/Desalination System Using Hydrophobic Membrane as an Energy Exchanger.” This project is supported by the Science & Engineering Research Board (SERB), Department of Science and Technology, Government of India, Project Number No. SR/20/ME/018.

## REFERENCES

1. Zhang, L.Z., 2012. Progress on heat and moisture recovery with membranes: From fundamentals to engineering applications. Energy Conversion and Management, 63, pp.173-195.
2. Bai, H., Zhu, J., Chen, Z. and Chu, J., 2018. State-of-art in modelling methods of membrane-based liquid desiccant heat and mass exchanger: A comprehensive review. International Journal of Heat and Mass Transfer, 125, pp.445-470.
3. Li, W. and Yao, Y., 2021. Thermodynamic analysis of internally cooled membrane-based liquid desiccant dehumidifiers of different flow types. International Journal of Heat and Mass Transfer, 166, p.120802.
4. Saraireh, M., 2012. Heat transfer and condensation of water vapour from humid air in compact heat exchangers (Doctoral dissertation, Victoria University).
5. Naik, B.K. and Muthukumar, P., 2021. Parametric and Performance Investigations on Novel Multipurpose Liquid Desiccant Drying/Desalination System. Heat Transfer Engineering, 42(13-14), pp.1142-1158.

6. Naik, B.K., Chinthala, M., Patel, S. and Ramesh, P., 2021. Performance assessment of waste heat/solar driven membrane-based simultaneous desalination and liquid desiccant regeneration system using a thermal model and KNN machine learning tool. Desalination, 505, p.114980.
7. Min, J., Hu, T. and Liu, X., 2010. Evaluation of moisture diffusivities in various membranes. Journal of Membrane Science, 357(1-2), pp.185-191.
8. Bai, H., Zhu, J., Chen, Z. and Chu, J., 2018. Parametric analysis of a crossflow membrane-based parallel-plate liquid desiccant dehumidification system: numerical and experimental data. Energy and Buildings, 158, pp.494-508.
9. Naik, B.K., Muthukumar, P. and Bhattacharyya, C., 2019. Thermal modelling and parametric investigations on coupled heat and mass transfer processes occurred in a packed tower. Heat and Mass Transfer, 55(3), pp.627-644.
10. Naik, B.K., Singh, B., Dutta, N., Subbiah, S. and Muthukumar, P., 2020. Fluid to liquid membrane energy exchanger for simultaneous liquid desiccant regeneration and desalination applications–Theoretical and experimental analyses. Energy Conversion and Management, 204, p.112291.
11. M. Conde Engineering., 2004. Thermophysical properties of LiCl – H2O solutions, www.mrc-eng.com.
12. Hu J, Kim C, Halasz P, Kim JF, Kim J, Szekely G. Artificial intelligence for performance prediction of organic solvent nanofiltration membranes. J. Memb. Sci. 2021;619:118513. https://doi.org/10.1016/j.memsci.2020.118513.
13. Tan HH, Lim KH. Review of second-order optimization techniques in artificial neural networks backpropagation. IOP Conf. Ser. Mater. Sci. Eng. 2019;495: 012003. https://doi.org/10.1088/1757-899X/495/1/012003.
14. Coulibaly P, Bob´ee B, Anctil F. Improving extreme hydrologic events forecasting using a new criterion for artificial neural network selection. Hydrol Process 2001; 15(8):1533–6. https://doi.org/10.1002/hyp.v15:810.1002/hyp.445.
15. Coulibaly P, Anctil F, Bob´ee B. Multivariate Reservoir Inflow Forecasting Using Temporal Neural Networks. J Hydrol Eng 2001;6(5):367–76. https://doi.org/ 10.1061/(ASCE)1084-0699(2001)6:5(367).
16. Coulibaly P, Anctil F, Aravena R, Bob´ee B. Artificial neural network modeling of water table depth fluctuations. Water Resour Res 2001;37(4):885–96. https://doi. org/10.1029/2000WR900368.
17. Toth E, Brath A, Montanari A. Comparison of short-term rainfall prediction models for real-time flood forecasting. J Hydrol 2000;239(1-4):132–47. https://doi.org/ 10.1016/S0022-1694(00)00344-9.
18. M.K. Transtrum, J.P. Sethna, Improvements to the Levenberg-Marquardt algorithm for nonlinear least-squares minimization, (2012). http://arxiv.org/abs/1201.5885.
19. Sharma B, Venugopalan PK. Comparison of Neural Network Training Functions for Hematoma Classification in Brain CT Images. IOSR J Comput Eng 2014;16(1): 31–5. https://doi.org/10.9790/0661-16123135.
20. Ranade NV, Nagarajan S, Sarvothaman V, Ranade VV. ANN based modelling of hydrodynamic cavitation processes: Biomass pre-treatment and wastewater treatment. Ultrason Sonochem 2021;72:105428. https://doi.org/10.1016/j. ultsonch.2020.105428.
21. Lee S, Kim J. Prediction of Nanofiltration and Reverse-Osmosis-Membrane Rejection of Organic Compounds Using Random Forest Model. J Environ Eng 2020; 146(11):04020127. https://doi.org/10.1061/(ASCE)EE.1943-7870.0001806.
22. Yeo CSH, Xie Q, Wang X, Zhang S. Understanding and optimization of thin film nanocomposite membranes for reverse osmosis with machine learning. J. Memb. Sci. 2020;606:118135. https://doi.org/10.1016/j.memsci.2020.118135.
23. Skumanich A, Mints P, Ghiassi M. Considerations for the use of PV and PT for sea water desalination: The viability of floating solar for this application. In: Conference Record of the IEEE Photovoltaic Specialists Conference 2020-June; 2020. p. 0633–5. https://doi.org/10.1109/PVSC45281.2020.9300446.
24. Nazif S, Mirashrafi E, Roghani B, Bidhendi GN. Artificial Intelligence-Based Optimization of Reverse Osmosis Systems Operation Performance. J Environ Eng 2020;146(2):04019106. https://doi.org/10.1061/(ASCE)EE.1943-7870.0001613.
25. Babanezhad M, Masoumian A, Nakhjiri AT, Marjani A, Shirazian S. Influence of number of membership functions on prediction of membrane systems using adaptive network based fuzzy inference system (ANFIS). Sci Rep 2020;10(1). https://doi.org/10.1038/s41598-020-73175-0.
26. Soleimanzade MA, Sadrzadeh M. Deep learning-based energy management of a hybrid photovoltaic-reverse osmosis-pressure retarded osmosis system. Appl Energy 2021;293:116959. https://doi.org/10.1016/j.apenergy.2021.116959.

27. Faegh M, Behnam P, Shafii MB, Khiadani M. Development of artificial neural networks for performance prediction of a heat pump assisted humidification-dehumidification desalination system. Desalination 2021;508:115052. https://doi. org/10.1016/j.desal.2021.115052.
28. Rath, R., Dutta, D., Kamesh, R., Sharqawy, M.H., Moulik, S. and Roy, A., 2022. Rational design of high-power density “Blue Energy Harvester” pressure retarded osmosis (PRO) membranes using artificial intelligence-based modeling and optimization. Energy Conversion and Management, 253, p.115160.
29. Yu, H. and Wilamowski, B.M., 2011. Levenberg-marquardt training. Industrial electronics handbook, 5(12), p.1.
30. Burden, F. and Winkler, D., 2008. Bayesian regularization of neural networks. Artificial neural networks, pp.23-42.